

University of Dundee

The effect of Fe-acceptor doping on the electrical properties of $\text{Na}_{1/2}\text{Bi}_{1/2}\text{TiO}_3$ and $0.94 (\text{Na}_{1/2}\text{Bi}_{1/2})\text{TiO}_3 - 0.06 \text{BaTiO}_3$

Steiner, Sebastian; Seo, In Tae; Ren, Pengrong; Li, Ming; Keeble, David J.; Frömling, Till

Published in:
Journal of the American Ceramic Society

DOI:
[10.1111/jace.16401](https://doi.org/10.1111/jace.16401)

Publication date:
2019

Document Version
Peer reviewed version

[Link to publication in Discovery Research Portal](#)

Citation for published version (APA):

Steiner, S., Seo, I. T., Ren, P., Li, M., Keeble, D. J., & Frömling, T. (2019). The effect of Fe-acceptor doping on the electrical properties of $\text{Na}_{1/2}\text{Bi}_{1/2}\text{TiO}_3$ and $0.94 (\text{Na}_{1/2}\text{Bi}_{1/2})\text{TiO}_3 - 0.06 \text{BaTiO}_3$. *Journal of the American Ceramic Society*, 102(9), 5295–5304. <https://doi.org/10.1111/jace.16401>

General rights

Copyright and moral rights for the publications made accessible in Discovery Research Portal are retained by the authors and/or other copyright owners and it is a condition of accessing publications that users recognise and abide by the legal requirements associated with these rights.

- Users may download and print one copy of any publication from Discovery Research Portal for the purpose of private study or research.
- You may not further distribute the material or use it for any profit-making activity or commercial gain.
- You may freely distribute the URL identifying the publication in the public portal.

Take down policy

If you believe that this document breaches copyright please contact us providing details, and we will remove access to the work immediately and investigate your claim.

Article type : Article

The effect of Fe-acceptor doping on the electrical properties of $\text{Na}_{1/2}\text{Bi}_{1/2}\text{TiO}_3$ and 0.94 $(\text{Na}_{1/2}\text{Bi}_{1/2})\text{TiO}_3$ -0.06 BaTiO_3

Sebastian Steiner¹, In-Tae Seo¹, Pengrong Ren^{1,2}, Ming Li³, David J. Keeble⁴, Till Frömling^{*1}

¹Institute of Materials Science, Technische Universität Darmstadt, FB Nichtmetallisch-Anorganische Werkstoffe, Alarich-Weiss-Straße 2, 64287 Darmstadt, Germany

²Shaanxi Province Key Laboratory for Electrical Materials and Infiltration Technology, School of Materials Science and Engineering, Xi'an University of Technology, NO.5 South Jinhua Road, Xi'an, 710048, China

³Department of Mechanical, Materials and Manufacturing Engineering, University of Nottingham, Nottingham, NG7 2RD, UK

⁴School of Science and Engineering, University of Dundee, Dundee DD1 4HN, Scotland, UK

*corresponding author: Till Frömling froemling@ceramics.tu-darmstadt.de

Abstract:

$\text{Na}_{1/2}\text{Bi}_{1/2}\text{TiO}_3$ (NBT) based ceramics are amongst the most promising lead-free ferroelectric materials. It was expected that the defect chemistry and the effect of doping of NBT would be similar to that observed for lead based materials, however, acceptor doping does not lead to ferroelectric hardening. Instead, high oxygen ionic conductivity is induced. Nevertheless, for solid solutions with BaTiO_3 (BT), which are more relevant with respect to ferroelectric applications, such a drastic change of electrical properties has not been observed so far. To rationalize the difference in defect chemistry between NBT and its solid solution 94 $(\text{Na}_{1/2}\text{Bi}_{1/2})\text{TiO}_3$ -0.06 BaTiO_3 (NBT-6BT) compositions with different concentrations of Fe-dopant were investigated. The study illustrates that the materials exhibit very similar behavior to NBT, and extraordinarily high oxygen ionic conductivity could also be

This is the peer reviewed version of the following article: Steiner, S., et al. "The effect of Fe-acceptor doping on the electrical properties of $\text{Na}_{1/2}\text{Bi}_{1/2}\text{TiO}_3$ and 0.94 $(\text{Na}_{1/2}\text{Bi}_{1/2})\text{TiO}_3$ -0.06 BaTiO_3 ", *Journal of the American Ceramic Society* (2019), which has been published in final form at <https://doi.org/10.1111/jace.16401>. This article may be used for non-commercial purposes in accordance with Wiley Terms and Conditions for Self-Archiving.

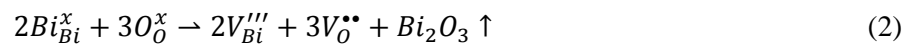
This article is protected by copyright. All rights reserved.

of ionic conductivity with dopant concentration. Previous studies of NBT-6BT have not reached sufficiently high dopant concentrations to observe high conductivity. In consequence, the same defect chemical model can be applied to both NBT and its solid solutions. This will help to rationalize the effect of doping on ferroelectric properties of NBT-ceramics and defect chemistry related degradation and fatigue.

Introduction:

Acceptor doping of ferroelectric materials is known to cause a “hardening” effect on the ferroelectric properties(1-4). This effect has often been reported for Fe^{3+} ions occupying the Ti^{4+} B-sites in lead zirconate titanate ($Pb(Zr,Ti)O_3$, PZT) or $BaTiO_3$ perovskites and is related to the formation of defect dipoles between the Fe acceptor ion and the charge compensating oxygen vacancies.(5-7) These defect dipoles induce a time dependent clamping of the domain wall motion and, in consequence, lead to ferroelectric hardening.(5, 8)

For the lead-free ferroelectric ceramic sodium bismuth titanate ($Na_{1/2}Bi_{1/2}TiO_3$, NBT) it can generally be expected that oxygen vacancies are induced by acceptor doping or bismuth off-stoichiometry:(9-11)



Eq. (1) is an example of an acceptor doping reaction and Eq. (2) represents the evaporation of Bi_2O_3 . Thus oxygen vacancies can be generated by either acceptor doping or bismuth non-stoichiometry. In PZT and $BaTiO_3$ based ceramics defect complexes such as $(Fe'_{Ti} - V_O^{\bullet\bullet})^{\bullet}$ are formed and oxygen vacancies are thus not mobile. For NBT, however, acceptor doping can lead to an unexpectedly high ionic conductivity. Studies by Li *et al.* reported a 4 orders of magnitude higher ionic conductivity in Mg B-site acceptor doped as well as slightly non-stoichiometric (1 mol% Bi-deficiency) NBT.(9, 10) The conductivity is even in the range of excellent oxygen ionic conductors like yttria stabilized zirconia (YSZ). This is highly detrimental for piezoelectric applications and illustrates that knowledge of the defect chemical properties of lead-based ferroelectrics cannot be directly transferred to the lead-free successors. However, evidence has been provided that the complex formation in NBT is highly dependent on dopant concentration, or oxygen vacancy concentration, respectively.(9-13) The higher the dopant concentration, the higher the concentration of mobile oxygen vacancies. The dependence of complex formation on vacancy concentration can be expected to be non-linear as the ionic conductivity changes by orders of magnitude with only small changes in acceptor concentration.(13) Furthermore, the conductivity is affected by the temperature dependent changes in the crystal structure as well as by a coexistence of phases in NBT.(13-15) The resulting non-linear dependence of

conductivity on defect concentration is in stark contrast to other common ceramics. The conductivity σ is actually expected to increase linearly with oxygen vacancy concentration:

$$\sigma = ze [V_O^{\bullet\bullet}] \mu(T) \quad (3)$$

where $\mu(T)$ is the temperature dependent vacancy mobility, $[V_O^{\bullet\bullet}]$ the oxygen vacancy concentration and ze the vacancy charge. There are other examples of changes in migration barrier height with high acceptor dopant concentration leading to a deviation of the linear relationship.(16, 17) However, the impact on conductivity is by far not as extensive and the low temperature conductivity is hardly affected. In case of NBT the conductivity changes from low intrinsic electronic conductivity to orders of magnitude higher ionically dominated conductivity with small acceptor content variations over a wide temperature range.(13) With respect to the ferroelectric properties it could be shown that high dielectric loss and leakage current results with high oxygen vacancy content already at room temperature.(18) Compositions for which polarization loops could be obtained did not show a hardening effect. The remanent polarization, however, could be indirectly modified by the influence of defects on grain size. The size of the grains has a profound impact on the dominant relaxor phases.(18)

For ferroelectric applications pure NBT is less relevant, the solid solution $0.94(\text{Na}_{1/2}\text{Bi}_{1/2}\text{TiO}_3)$ - 0.06BaTiO_3 (NBT-6BT) is at the morphotropic phase boundary and thus exhibits superior ferroelectric properties.(19-21) The data on the impact of Bi-deficiency on NBT-BT is rather ambiguous. In one previous study it was found that NBT-6BT is significantly less sensitive to the generation of ionic conductivity with A-site non-stoichiometry than NBT.(22) The dielectric loss increases but generally only the ferroelectric properties are modified. Different synthesis procedures lead to different bismuth evaporation and hence defect concentration (Eq. 2). Thus, this could also explain a rather large spread of reported properties of NBT-BT in literature. However, Prasertpalichat *et al.* provided evidence of high ionic conductivity in off-stoichiometric NBT-BT.(23) Nevertheless, Sapper *et al.* even reported that ferroelectric hardening in NBT-6BT is possible by a B-site Fe acceptor doping.(24) It has also been shown that A-site acceptor doping introduced by A-site non-stoichiometry can induce hardening.(25) The extent of hardening was, however, reduced from that expected using the knowledge of lead-containing ceramics. Recently, it was even shown that by controlling A-site stoichiometry it is possible to produce NBT-BT material with very low dielectric loss up to almost 400°C. This extraordinarily resistive dielectric is amongst the most promising materials for high temperature capacitor applications.(26) In consequence, it can be seen that the properties of NBT-based materials range from highly ionically conductive to highly resistive. Such a wide spread of properties of a ceramic is quite unique, even accounting for variations due to the formation of the solid solutions. On the one hand, this makes NBT-based material interesting for various applications, on the other hand it highlights the lack of an understanding of the defect chemical origin for this large

property range. So far we do not even have enough information to explain the effect of defects on the favored primary ferroelectric properties. For example, it could be shown that changes in the A-site stoichiometry significantly impact the microstructure of NBT solid solutions which additionally influences ferroelectric properties. In NBT solutions with strontium titanate the development of core-shell structures could be controlled, which changed ferroelectric parameters drastically.(27) It is currently not possible to predict secondary properties such as degradation and fatigue.(28) In consequence, investigations that provide insight on the mechanisms responsible for this unusual behavior are of particular importance.

In this study, the effects of B-site Fe acceptor doping on the electrical conductivity of NBT and NBT-6BT are investigated, and compared. It provides evidence that suggests the defect chemical approaches, which have already been established for pure NBT, can also be applied to the technologically relevant complex solid solutions. A main focus of the study was to investigate the relation between acceptor dopant induced oxygen vacancies and their effect on the electrical conductivity. To avoid undesired high leakage current due to low levels of Bi deficiency, especially in the NBT compositions, a small Bi-excess (0.2 mol%) was added to the nominal starting compositions.

Experimental

Polycrystalline samples of $\text{Na}_{0.5}\text{Bi}_{0.501}\text{TiO}_3$ (NBT), and $\text{Na}_{0.5}\text{Bi}_{0.501}\text{Fe}_x\text{Ti}_{1-x}\text{O}_3$ ($x=0.001, 0.003, 0.01, 0.02, 0.03$, and 0.04) as well as $0.94\text{Na}_{0.5}\text{Bi}_{0.501}\text{Fe}_x\text{Ti}_{1-x}\text{O}_3-0.06\text{BaTiO}_3$ ($x=0.01, 0.02, 0.03$, and 0.04) were prepared using the conventional solid oxide synthesis route with reagent oxides and carbonates (Alfa Aesar GmbH & Co. KG). Na_2CO_3 (99.5%), Bi_2O_3 (99.975%), TiO_2 (99.6%), BaCO_3 (99.8%) and Fe_2O_3 (99.5%) were used as raw materials and have been dried in an oven (Nabertherm, HTC 08/15) at 180°C (Bi_2O_3), 300°C (Na_2CO_3 , Fe_2O_3 , BaCO_3) and 1000°C (TiO_2), for 8 h before weighing to avoid non-stoichiometry caused by hygroscopic carbonates.(10) Furthermore, to avoid the formation of additional Bi vacancies and corresponding oxygen vacancies during the processing, all Fe-doped starting compositions exhibit a small Bi-excess of 0.2 mol% as the volatilization temperature of Bi_2O_3 ($T>825^\circ\text{C}$) is considerably lower than for Na_2O ($T>1132^\circ\text{C}$). (29) All the weighed powders were submerged in ethanol and ball milled in a planetary ball mill (Fritsch, Pulverisette 5) for 6 h using yttria stabilized zirconia balls (diameter 10 mm; ratio 10:1). Afterwards, the dried powders were calcined in a covered alumina crucible at 800°C for 2 h. To guarantee a homogeneous distribution, the calcined powders were ball milled again for 4 h and calcined a second time at 850°C for 2 h followed by ball milling over 6 h to enable a full reaction of the raw materials. The prepared powders have been uniaxially compacted into pellets (diameter 10 mm) with a pressure of ca. 25 MPa and pressed cold isostatically at 200 MPa (Weber, KIP 100E). Finally, the pressed NBT and NBT-6BT pellets were sintered at 1150°C for 2 h at a heating rate of 5 K/min.

The phase and purity of the prepared compositions have been investigated via X-ray diffraction (XRD) using $Cu_{K\alpha}$ radiation (Bruker AXS D8 Advance). Grain size as well as the possible formation of secondary phases have been investigated via scanning electron microscopy (SEM) (JEOL, Model JSM 7600F, Japan) in the SE (samples thermally etched at 1100°C for 5 minutes and sputtered with gold) and back-scattered electron (BSE) (samples sputtered with carbon) mode with additional energy dispersive X-ray (EDX) analysis (Oxford Link ISIS, Oxford Instruments Ltd., Oxfordshire, UK). With the help of a Novocontrol alpha A impedance analyzer (Novocontrol, Montabaur, Germany), the temperature and frequency dependent impedance was determined. The frequency range of the probing signal was set between 0.1 Hz and 3 MHz with an amplitude of 0.1 V. The investigations were conducted in a temperature range between 150°C and 700°C with a step size of 10 K. For the analysis of the generated impedance results, the RelaxIS software (rhd instruments, Darmstadt, Germany) was used. The ferroelectric polarization at room temperature has been investigated at 1 Hz and an electric field up to 8 kV/mm (high voltage amplifier TREK model 20/20C, Trek Inc., USA). Furthermore, oxygen ion transport numbers were determined by electromotive force measurements (EMF) with a ProboStat system (NorECs Norwegian Electro Ceramics AS, Oslo, Norway). The ceramic pellet was sealed onto a YSZ tube using a commercial glass frit. An oxygen partial pressure, pO_2 , difference was created across the ceramic by flowing N_2 into the YSZ tube and leaving the outside of the ceramic in air. The pO_2 difference was monitored by measuring the voltage across the inner and outer electrodes on the YSZ tube. The voltage was measured using a Solartron Schlumberger 7150 digital multimeter.

Results and Discussion

Figure 1 shows the XRD patterns of 0.1-4 mol% Fe doped as well as pure NBT and 1-4 mol% Fe doped NBT-6BT ceramics. All ceramics are consistent with the room temperature R3c-group structure.(14, 30, 31) However, if the amount of Fe_2O_3 doping exceeds 1 mol% for NBT or 3 mol% for NBT-6BT, secondary phases (denoted by stars, see Figure 1) can be detected. Additional EDX analysis revealed that this secondary phase is a Fe-, Ti-rich and Bi-deficient phase (see supporting information Figure S1). It can be concluded that the solubility limit for Fe-doping is reached in NBT between 1 and 2 mol% and in NBT-6BT between 3 and 4 mol%, respectively. SEM analysis was carried out to elucidate the morphology of the secondary phases (BSE mode) and to investigate the influence of defect concentrations on the microstructure (secondary electron mode SE).

Figure 2 depicts the microstructures of pure NBT and NBT-6BT (Figure 2(a) and (b)) and 4 mol% Fe-doped NBT and NBT-6BT (Figure 2(c) and (d)) (SE and BSE images of the other processed compositions are given in the supporting information Figure S1). The Fe-acceptor doping shows a significant impact on the grain growth in both cases. The phenomenon has been previously attributed to the presence of increased oxygen vacancy concentration in literature. Higher oxygen vacancy concentration is expected to impact the grain boundary migration energy which leads to enhanced

grain growth.(22, 32-34) The insets in Figure 2(c) and (d) represent backscattered electron images of the 4 mol% Fe-doped compositions with highlighted secondary phases.

The grain size analysis for all processed compositions is summarized in Figure 3. Both ceramics provide a very similar grain size without Fe-doping (pure NBT $\sim 3\mu\text{m}$, pure NBT-6BT $\sim 2\mu\text{m}$). By adding only 0.1 mol% Fe, NBT shows an increase of about 400% in grain size. At 1 mol% Fe-doping the grain coarsening is about 800% with respect to pure NBT. NBT-6BT also shows grain coarsening but the effect is significantly smaller. Figure 3 also illustrates that a maximum grain size is obtained for 3 mol% Fe-doped NBT (grain size $\sim 33\mu\text{m}$). Due to the occurrence of secondary phases, the oxygen vacancy concentration in the matrix material may be reduced and thus additional grain coarsening could be inhibited.(35) Furthermore, the grain growth mechanism can be impacted by the secondary phase itself. The strong dependence of grain size with doping content is clearly shown in Figure 3. The formation of a solid solution, for instance with BaTiO_3 , seems to buffer against grain coarsening. According to previous reports, immobile oxygen vacancies can reduce grain boundary mobility.(36, 37)

Electron paramagnetic resonance (EPR) results from the 1, 2, and 4 % Fe doped NBT and NBT-6BT powdered ceramic samples are depicted in Figure 4. The low field resonance line at approximately 150 mT is characteristic of Fe^{3+} centers in a strongly axial crystal field exhibiting a large second order zero field splitting and can be attributed to Fe^{3+} nearest neighbor oxygen vacancy complex defects, $(\text{Fe}'_{\text{Ti}} - \text{V}_\text{O}^{\bullet\bullet})^\bullet$.(38) This resonance can be observed from all the samples studied. The weaker line observed in the 1% doped NBT sample centered at approximately 330 mT can be attributed to B-site substituted Fe^{3+} centers within complete oxygen octahedra. However, at higher Fe concentrations the line shape of the EPR line in the 300 mT region broadens markedly. The EPR of Fe_2O_3 and from Fe containing impurity phases exhibit similar broad resonances.(1, 39) The spectra observed from the 2 % and 4 % Fe doped NBT samples are consistent with an increasing contribution for EPR spectra from Fe-containing impurity phases. The spectral contribution in the region of 300 mT observed from the 2 % and 4 % Fe doped NBT-6BT samples (Fig. 4b) can also be attributed to Fe-containing impurity phases. The spectrum from the 4 % doped sample clearly exhibits two contributions in this field region, the additional narrow line is likely due to an impurity phase in which the Fe centers are exhibiting exchange narrowing. The onset of the detection of a broadened spectrum in the approximate region of 300 mT for 2 % Fe in NBT is consistent with the detection of Fe-rich secondary phases by XRD (Figure 1(a)). For NBT-6BT a secondary phase was detected by XRD in the 4% Fe and there is a dominant contribution from a Fe-containing impurity phase in the EPR (Figure 4(b)). For the NBT samples contribution from $(\text{Fe}'_{\text{Ti}} - \text{V}_\text{O}^{\bullet\bullet})^\bullet$ centers increases on increasing from 1 % to 2 % Fe, however no further increase is evident for the 4 % Fe doped sample. The contribution from the $(\text{Fe}'_{\text{Ti}} - \text{V}_\text{O}^{\bullet\bullet})^\bullet$ centers does not markedly change for the Fe doped NBT-6BT samples.

The variation in grain size with Fe-doping shown in Figure 3 provides evidence for the presence and importance of oxygen vacancies, while the EPR results demonstrate the existence of $(Fe_{Ti}' - V_O^{\bullet\bullet})^{\bullet}$ centers for both materials. Information on the mobility of the oxygen vacancies involved is required to further elucidate the difference between NBT and NBT-6BT. To achieve this, the impact of doping on the electrical properties will be discussed in the following. Figure 5 shows the Nyquist plots (imaginary part $-Z''$ plotted against real part Z' of impedance) from impedance spectroscopy (IS) data of Fe doped NBT and NBT-6BT measured from 0.1 Hz to 3 MHz at 500°C. In the case of pure NBT, 0.1 and 0.3 mol% Fe doped NBT and pure as well as 1 mol% Fe-doped NBT-6BT only one single semicircle and therefore a single conduction process can be detected within the measuring frequency range ($R_b \sim 1.2 \text{ M}\Omega\text{cm}$ at 500°C). This is well in line with recently reported results on Mg-acceptor doped NBT.(13) Low concentrations of acceptor dopant do not lead to a significant increase in conductivity and the conductivity is dominated by an intrinsic electronic contribution. However, a non-linear increase in conductivity can be observed with increasing the concentration to 1% for pure NBT. Two semicircles start to form in this case. The high frequency process represents the bulk ($R_b \sim 1 \text{ k}\Omega\text{cm}$ at 500°C), the lower frequency process the grain boundary response ($R_{gb} \sim 2.5 \text{ k}\Omega\text{cm}$ at 500°C). The tail after the second process is a typical feature of Warburg-type diffusion of oxygen ions at the sample/electrode interface.(40) This is already a hint towards a dominating ionic conductivity and hence a change in primary conduction process with increasing acceptor concentration. When the doping level reaches 2 mol% Fe, the total conductivity of all samples again increases by one additional order of magnitude until it saturates above a 2 mol% doping content. This finding again coincides well with recent findings on other acceptor dopants in NBT.(12)

The Fe doped NBT-6BT ceramics show a comparable behavior to NBT. A clear transition from low to high conductivity can be observed in Figure 5(b). The conductivity values also coincide well with the NBT conductivity, which is in the range of excellent oxygen electrolytes like YSZ. This is rather unexpected given that NBT-BT has been discussed so far to be different to NBT with respect to conductivity. However, the transition towards higher conductivity occurs at a higher acceptor dopant concentration. For NBT-6BT the 1 mol% doped sample still exhibits a quite low conductivity with only one visible semi-circle. NBT is already highly conductive in this case (see comparison in Figure 5 (c)). More details are revealed by investigation of Arrhenius type plots of the conductivity which are represented in Figure 6. From the slope of the Arrhenius plot the activation energy of conduction processes has been calculated. Pure NBT has a low bulk conductivity. The activation energy changes from low values (0.92eV) to high values (1.54eV) by increasing the temperature. This phenomenon represents a change from extrinsic (lower T) to intrinsic (higher T) semiconducting behavior. In the low temperature region, extrinsic semiconducting behavior is dominant with lower activation energies. The origin of a decreased activation energy can be attributed to additional energy levels within the band gap caused by impurity states. In contrast, the high activation energy, observed at elevated temperatures, represents a value close to half of the band gap of NBT ($E_{bg} \sim 3.3 \text{ eV}$) which

Accepted Article
demonstrates an almost ideal intrinsic electronic behavior.(41) The 0.1 and 0.3 mol% Fe-doped NBT compositions also show a relatively low total conductivity. A small decrease in the activation energies compared to pure NBT can be explained by an increased level of defect states within the band gap. These could of course result from a higher concentration of oxygen vacancies. However, at higher concentrations the oxygen vacancies are responsible for the dominant ionic conductivity. This behavior has already been reported as a typical feature of NBT based B-site acceptor doped oxygen ionic conductors and was attributed to a phase and defect dipole formation dependent concentration of mobile vacancies.(12, 13) The total conductivity increases by at least four orders of magnitude over the whole temperature range and saturates for doping levels above 2 mol% Fe. Moreover, the activation energy of the bulk conduction process changes from higher values (~0.86 eV) to lower values (~0.43-0.51 eV) with increasing the temperature. With regards to an increased doping level above 2 mol%, the bulk conductivity is not going to be further increased (see Figure 6). As discussed above, the solubility of Fe_2O_3 is limited to less than 2 mol%. Therefore, the induced oxygen vacancy concentration did not change any further, even by increasing the doping level. Furthermore, the conductivity is already in a range for which a general limit of oxygen ion conductivity is expected in perovskites.(35, 42) Thus, irrespective of dopant solubility limit the conductivity is not expected to be further increased significantly.

The similar behavior of Fe doped NBT-6BT compositions is again illustrated in the Arrhenius plots in Figure 6(b). The differently doped NBT-6BT compositions show highly resistive as well as highly conductive properties. Pure NBT-6BT as well as 1 mol% Fe-doped NBT-6BT show typical semiconducting behavior. By doping at least 2 mol% Fe, the conductivity jumps several orders of magnitude. A further increase in Fe doping content leads again to a saturation of the conductivity while showing a behavior which is usually attributed to oxygen ionic conductivity. Based on these results, we can suppose that the induced oxygen vacancy concentration by Fe-doping has a significant impact on the conduction mechanisms in NBT as well as NBT-6BT. Semiconducting behavior is dominant at low oxygen vacancy concentrations, while oxygen ionic conduction becomes dominant when additional oxygen vacancies are generated by the acceptor doping. As already seen for the grain coarsening effect, the formation of a solid solution with BT buffers the impact of an increased oxygen vacancy concentration compared to NBT with the same doping levels. It nevertheless does not completely change the defect concentration dependent behavior. To further prove that the high conductivity can be attributed to oxygen ionic conductivity the oxygen ionic transport numbers are obtained from electromotive force (EMF) measurements. These quantify the oxygen ionic conductivity contribution to the total conductivity and are shown for characteristic compositions (see Table 1).(9) According to recent simulations provided by Zhang *et al.* a high level of cation conductivity can be neglected in NBT.(43) As expected, the measured doped NBT samples (1% Fe and above) all exhibit dominating oxygen ionic conductivity. The 1 mol% Fe-doped NBT-6BT composition, however, shows a low ionic transport number of ~0.07 at 700°C and 800°C. This again

illustrates that even though there is a small change in conductivity from NBT-6BT to 1 mol% doped material the conduction mechanism is still dominated by electronic conductivity. The additional defects most likely rather act as traps for electronic charges leading to the extrinsic electronic contribution.(44, 45)

Even though Fe doped NBT and NBT-6BT show a similar conduction behavior, the needed vacancy concentration for dominant oxygen ionic conductivity differs. The NBT-6BT becomes less sensitive towards increasing vacancy concentration. This explains why reports on extraordinarily high conductivity in NBT-6BT are so rare.(23) The bismuth non-stoichiometry in NBT-6BT investigated for example by Seo *et al.* is not high enough to induce high ionic conductivity.(22) Similarly, it was possible for Sapper *et al.* to investigate ferroelectric hardening in 1 mol% Fe doped NBT-6BT.(24) The similarity in variation in structure, phase, and microstructure with Fe doped between NBT and NBT-6BT ceramics suggests the decrease in sensitivity of the conductivity to oxygen vacancies for NBT-6BT may be due to the A-site ion differences. The incorporation of a small fraction of Ba²⁺ ions at the A-site is the only obvious difference between NBT and NBT-6BT. The activation energy for oxygen ion migration in BaTiO₃ was reported to be around 1.0-1.1 eV.(46-48) The oxygen migration might be hindered in NBT-6BT ceramics due to a difference in the Bi-O and Ba-O bond strength. The Bi-O bonds might be weaker compared to Ba-O bonds.(49) It should be noted that the 1 mol% Fe doped NBT-BT showed lower ionic conductivity than the equivalently doped NBT. This will be an interesting starting point for further investigations.

The high field property differences between the doped NBT and NBT-6BT solid solutions will be of major interest. These affect general ferroelectric properties like remanent ferroelectric polarization P_r and coercive field E_c . Furthermore, they determine electrodegradation of the materials. In Figure 7 a first comparison of ferroelectric properties of NBT ceramics with different Fe concentrations are given. The figure illustrates the polarization plotted against the applied field at room temperature. For all depicted compositions regular ferroelectric polarization curves could be obtained. Even for the higher doped materials this is actually achievable without a sign of significant loss. Compared to previous literature about non-stoichiometric NBT compositions, these findings are rather surprising as a rather bulky and lossy loop would have been expected.(18) Hence, the low temperature resistance is high enough to allow for ferroelectric polarization switching. However, in case of the 2% doped NBT there was always a breakdown of electrical properties after a loop hinting towards a non-linear contribution of oxygen vacancies to the degradation of the material. A ferroelectric hardening should result in an increase of E_c and a lowering of the P_r value.(5-7) However, from regular NBT to 0.1% Fe doping there is actually an increase in P_r (Figure 7a)). This behavior is rather expected from donor doping or isovalent doping e.g. with Zr.(50) For Zr doping a stabilization of the ferroelectric order in the relaxor ferroelectric NBT-BT leads to this effect. Only at higher Fe-doping concentrations a hardening effect could be identified. This coincides with the onset of high ionic conductivity at higher temperatures. Thus, no hardening occurs in NBT material exhibiting semiconducting behavior over a

large temperature range, while mobile oxygen ionic defects contribute to a small hardening effect at higher concentrations. Nevertheless, it is unlikely that the small effect warrants taking the risk of mobile defects contributing non-linearly to loss increase and electrodegradation at room temperature. A similar behavior but less extensive can be observed for the NBT-6BT in Figure 7b). Furthermore, a generally lower E_c compared to pure NBT is found which is in line with previous research.(19-21) Thus, the point at which an immediate breakdown would occur for a highly Fe-doped NBT-6BT is not reached when recording a polarization curve in the range of E_c .

With the knowledge about the similarities and differences between NBT and its solid solutions with BT it is now possible to gain a general view on the defect chemistry of NBT-based material. This will eventually allow for further tuning of dielectric loss/conductivity and understanding the impact of defects on ferroelectric properties of NBT-ceramics which is obviously fundamentally different compared to lead based systems. Furthermore, this will help to elucidate mechanisms for degradation and fatigue which can be attributed to changes in defect chemistry. It can already be assumed that acceptor doping is generally detrimental to the long term stability of electrical properties of NBT-based materials.

Conclusion

The unusually high oxygen ionic conductivity previously observed in acceptor doped NBT can also be induced in acceptor doped solid solutions with BT. The changes in ionic conductivity are dependent on the defect concentration (oxygen vacancies and oxygen vacancy acceptor ion complexes) and can be rationalized by the same mechanisms. Values of ionic conductivity rivaling reported data for excellent oxygen conductors like yttria stabilized zirconia are found. This means that the defect chemistry of NBT, and of the far more technologically relevant NBT-6BT, exhibit more similarities than initially assumed. The difference is simply in the extent of the dependence of ionic conductivity on dopant/defect concentration. While NBT can already become highly ionically conductive at acceptor concentrations below 1%, NBT-6BT still exhibits low, mostly intrinsic, electronic conductivity. Only at higher acceptor concentrations NBT-6BT also becomes ionically conductive. Most of the previous studies on acceptor doping of NBT-6BT and impact of oxygen vacancies induced by Bi-deficiency have been performed on materials where the defect concentrations were below the threshold for extremely high ionic conductivity. Additionally, it is possible to obtain a high enough resistance at room temperature to achieve ferroelectric switching even in the ionically conductive materials. This knowledge will be important for rationalizing the impact of defects on electrical properties of NBT-based material in general. The minor hardening effect of ferroelectric properties can most likely be attributed to the unusual behavior of oxygen ionic defects in NBT materials. Furthermore, the point defect dependent electrical degradation and fatigue of ferroelectric NBT-ceramics can be expected to be very different compared to that observed in lead based ceramics.

Acknowledgements

The authors gratefully acknowledge financial support by the Deutsche Forschungsgemeinschaft (DFG) through project Grant No. FR 3718/1-1. Furthermore, the authors would like to thank Lalitha Kodumudi Venkataraman for her help with evaluating the ferroelectric data.

References

1. Aksel E, Erdem E, Jakes P, Jones JL, Eichel R-A. Defect structure and materials “hardening” in Fe_2O_3 -doped $[\text{Bi}_{0.5}\text{Na}_{0.5}]\text{TiO}_3$ ferroelectrics. *Applied Physics Letters*. 2010;97(1):012903.
2. Shrout TR, Zhang SJ. Lead-free piezoelectric ceramics: Alternatives for PZT? *Journal of Electroceramics*. 2007;19(1):113-26.
3. Boser O. Statistical theory of hysteresis in ferroelectric materials. *Journal of Applied Physics*. 1987;62(4):1344-8.
4. Robels U, Arlt G. Domain wall clamping in ferroelectrics by orientation of defects. *Journal of Applied Physics*. 1993;73(7):3454-60.
5. Carl K, Härdtl KH. Electrical after-effects in $\text{Pb}(\text{Ti}, \text{Zr})\text{O}_3$ ceramics. *Ferroelectrics*. 1977;17(1):473-86.
6. Arlt G, Neumann H. Internal bias in ferroelectric ceramics: Origin and time dependence. *Ferroelectrics*. 1988;87(1):109-20.
7. Lambeck PV, Jonker GH. Ferroelectric domain stabilization in BaTiO_3 by bulk ordering of defects. *Ferroelectrics*. 2011;22(1):729-31.
8. Arlt G, Robels U. Aging and fatigue in bulk ferroelectric perovskite ceramics. *Integrated Ferroelectrics*. 2006;3(4):343-9.
9. Li M, Pietrowski MJ, De Souza RA, Zhang H, Reaney IM, Cook SN, et al. A family of oxide ion conductors based on the ferroelectric perovskite $\text{Na}_{0.5}\text{Bi}_{0.5}\text{TiO}_3$. *Nature Materials*. 2014;13(1):31-5.
10. Li M, Zhang H, Cook SN, Li L, Kilner JA, Reaney IM, et al. Dramatic Influence of A-Site Nonstoichiometry on the Electrical Conductivity and Conduction Mechanisms in the Perovskite Oxide $\text{Na}_{0.5}\text{Bi}_{0.5}\text{TiO}_3$. *Chemistry of Materials*. 2015;27(2):629-34.
11. Yang F, Wu P, Sinclair DC. Enhanced bulk conductivity of A-site divalent acceptor-doped non-stoichiometric sodium bismuth titanate. *Solid State Ionics*. 2017;299:38-45.
12. Yang F, Li M, Li L, Wu P, Pradal-Velázquez E, Sinclair DC. Defect chemistry and electrical properties of sodium bismuth titanate perovskite. *Journal of Materials Chemistry A*. 2018;6(13):5243-54.
13. Koch L, Steiner S, Meyer K-C, Seo I-T, Albe K, Frömling T. Ionic conductivity of acceptor doped sodium bismuth titanate: influence of dopants, phase transitions and defect associates. *Journal of Materials Chemistry C*. 2017;5(35):8958-65.
14. Jones GO, Thomas PA. Investigation of the structure and phase transitions in the novel A-site substituted distorted perovskite compound $\text{Na}_{0.5}\text{Bi}_{0.5}\text{TiO}_3$. *Acta Crystallographica Section B*. 2001;B58:168-78.
15. Meyer K-C, Albe K. Influence of phase transitions and defect associates on the oxygen migration in the ion conductor $\text{Na}_{1/2}\text{Bi}_{1/2}\text{TiO}_3$. *Journal of Materials Chemistry A*. 2017.
16. Schie M, Waser R, De Souza RA. A Simulation Study of Oxygen-Vacancy Behavior in Strontium Titanate: Beyond Nearest-Neighbor Interactions. *The Journal of Physical Chemistry C*. 2014;118(28):15185-92.
17. Merkle R, Maier J. Defect association in acceptor-doped SrTiO_3 : case study for $\text{Fe}_{\text{Ti}}\text{V}_\text{O}$ and $\text{Mn}_{\text{Ti}}\text{V}_\text{O}$. *Physical Chemistry Chemical Physics*. 2003;5(11):2297-303.
18. Mishra A, Khatua DK, De A, Majumdar B, Frömling T, Ranjan R. Structural mechanism behind piezoelectric enhancement in off-stoichiometric $\text{Na}_{0.5}\text{Bi}_{0.5}\text{TiO}_3$ based lead-free piezoceramics. *Acta Materialia*. 2019;164:761-75.

19. Daniels JE, Jo W, Rödel J, Jones JL. Electric-field-induced phase transformation at a lead-free morphotropic phase boundary: Case study in a 93%($\text{Bi}_{0.5}\text{Na}_{0.5}$) TiO_3 –7%Ba TiO_3 piezoelectric ceramic. *Applied Physics Letters*. 2009;95(3):032904.
20. Jo W, Daniels JE, Jones JL, Tan X, Thomas PA, Damjanovic D, et al. Evolving morphotropic phase boundary in lead-free ($\text{Bi}_{1/2}\text{Na}_{1/2}$) TiO_3 –Ba TiO_3 piezoceramics. *Journal of Applied Physics*. 2011;109(1):014110.
21. Jo W, Schaab S, Sapper E, Schmitt LA, Kleebe H-J, Bell AJ, et al. On the phase identity and its thermal evolution of lead free ($\text{Bi}_{1/2}\text{Na}_{1/2}$) TiO_3 -6 mol% Ba TiO_3 . *Journal of Applied Physics*. 2011;110(7):074106.
22. Seo I-T, Steiner S, Frömling T. The effect of A site non-stoichiometry on 0.94(Na_yBi_x) TiO_3 -0.06Ba TiO_3 . *Journal of the European Ceramic Society*. 2017;37(4):1429-36.
23. Prasertpalichat S, Schmidt W, Cann DP. Effects of A-site nonstoichiometry on oxide ion conduction in 0.94 $\text{Bi}_{0.5}\text{Na}_{0.5}\text{TiO}_3$ –0.06Ba TiO_3 ceramics. *Journal of Advanced Dielectrics*. 2016;06(02):1650012.
24. Sapper E, Dittmer R, Damjanovic D, Erdem E, Keeble DJ, Jo W, et al. Aging in the relaxor and ferroelectric state of Fe-doped $(1-x)(\text{Bi}_{1/2}\text{Na}_{1/2})\text{TiO}_3$ -xBa TiO_3 piezoelectric ceramics. *Journal of Applied Physics*. 2014;116(10):104102.
25. Prasertpalichat S, Cann DP. Hardening in non-stoichiometric $(1-x)\text{Bi}_{0.5}\text{Na}_{0.5}\text{TiO}_3$ -xBa TiO_3 lead-free piezoelectric ceramics. *Journal of Materials Science*. 2016;51(1):476–86.
26. Höfling M, Steiner S, Hoang A-P, Seo I-T, Frömling T. Optimizing the defect chemistry of $\text{Na}_{1/2}\text{Bi}_{1/2}\text{TiO}_3$ -based materials: paving the way for excellent high temperature capacitors. *Journal of Materials Chemistry C*. 2018;6(17):4769-76.
27. Frömling T, Steiner S, Ayrikyan A, Breimecker D, Dürrschnabel M, Molina-Luna L, et al. Designing properties of $(\text{Na}_{1/2}\text{Bi}_x)\text{TiO}_3$ -based materials through A-site non-stoichiometry. *Journal of Materials Chemistry C*. 2018;6(4):738-44.
28. Koruza J, Bell AJ, Frömling T, Webber KG, Wang K, Rödel J. Requirements for the transfer of lead-free piezoceramics into application. *Journal of Materiomics*. 2018;4(1):13-26.
29. J. Carter EA, T. Iamsasri, J.S. Forrester, J. Chen, J.L. Jones. Structure and ferroelectricity of nonstoichiometric $(\text{Na}_{0.5}\text{Bi}_{0.5})\text{TiO}_3$. *Appl Phys Lett*. 2014;11(104).
30. Dorcet V, Trolliard G, Boullay P. Reinvestigation of Phase Transitions in $\text{Na}_{0.5}\text{Bi}_{0.5}\text{TiO}_3$ by TEM. Part I: First Order Rhombohedral to Orthorhombic Phase Transition. *Chemistry of Materials*. 2008;20(15):5061-73.
31. Trolliard G, Dorcet V. Reinvestigation of Phase Transitions in $\text{Na}_{1/2}\text{Bi}_{1/2}\text{TiO}_3$ by TEM. Part II: Second Order Orthorhombic to Tetragonal Phase Transition. *Chemistry of Materials*. 2008;20(15):5074-82.
32. Sung YS, Kim JM, Cho JH, Song TK, Kim MH, Park TG. Effects of Bi nonstoichiometry in $(\text{Bi}_{0.5+x}\text{Na}_{0.5-x})\text{TiO}_3$ ceramics. *Applied Physics Letters*. 2011;98(1):012902.
33. Qiao X-S, Chen X-M, Lian H-L, Chen W-T, Zhou J-P, Liu P. Microstructure and Electrical Properties of Nonstoichiometric 0.94($\text{Na}_{0.5}\text{Bi}_{0.5+x}$) TiO_3 –0.06Ba TiO_3 Lead-Free Ceramics. *Journal of the American Ceramic Society*. 2016;99(1):198-205.
34. Zuo R, Su S, Wu Y, Fu J, Wang M, Li L. Influence of A-site nonstoichiometry on sintering, microstructure and electrical properties of $(\text{Bi}_{0.5}\text{Na}_{0.5})\text{TiO}_3$ ceramics. *Materials Chemistry and Physics*. 2008;110(2–3):311-5.
35. Yang F, Li M, Li L, Wu P, Pradal-Velázquez E, Sinclair DC. Optimisation of oxide-ion conductivity in acceptor-doped $\text{Na}_{0.5}\text{Bi}_{0.5}\text{TiO}_3$ perovskite: approaching the limit? *Journal of Materials Chemistry A*. 2017;5(41):21658-62.
36. Jung Y, Choi S, Kang S. Effect of oxygen partial pressure on grain boundary structure and grain growth behavior in Ba TiO_3 . *Acta Materialia*. 2006;54(10):2849-55.
37. An S-M, Kang S-JL. Boundary structural transition and grain growth behavior in Ba TiO_3 with Nd_2O_3 doping and oxygen partial pressure change. *Acta Materialia*. 2011;59(5):1964-73.

38. Kirkpatrick ES, Müller KA, Rubins RS. Strong Axial Electron Paramagnetic Resonance Spectrum of Fe^{3+} in SrTiO_3 Due to Nearest-Neighbor Charge Compensation. *Physical Review*. 1964;135(1A):A86-A90.
39. Kleebe H-J, Lauterbach S, Silvestroni L, Kungl H, Hoffmann MJ, Erdem E, et al. Formation of magnetic grains in ferroelectric $\text{Pb}[\text{Zr}_{0.6}\text{Ti}_{0.4}]\text{O}_3$ ceramics doped with Fe^{3+} above the solubility limit. *Applied Physics Letters*. 2009;94(14):142901.
40. Maier RA, Randall CA, Stevenson J. Low-Temperature Ionic Conductivity of an Acceptor-Doped Perovskite: I. Impedance of Single-Crystal SrTiO_3 . *Journal of the American Ceramic Society*. 2016;99(10):3350-9.
41. Bousquet M, Duclère JR, Orhan E, Boule A, Bachelet C, Champeaux C. Optical properties of an epitaxial $\text{Na}_{0.5}\text{Bi}_{0.5}\text{TiO}_3$ thin film grown by laser ablation: Experimental approach and density functional theory calculations. *Journal of Applied Physics*. 2010;107(10):104107.
42. De Souza RA. Oxygen Diffusion in SrTiO_3 and Related Perovskite Oxides. *Advanced Functional Materials*. 2015;25(40):6326-42.
43. Zhang H, Ramadan AHH, De Souza RA. Atomistic simulations of ion migration in sodium bismuth titanate (NBT) materials: towards superior oxide-ion conductors. *Journal of Materials Chemistry A*. 2018;6(19):9116-23.
44. Warren WL, Dimos D, Pike GE, Vanheusden K, Ramesh R. Alignment of defect dipoles in polycrystalline ferroelectrics. *Applied Physics Letters*. 1995;67(12):1689-91.
45. Meštrić H, Eichel RA, Kloss T, Dinse KP, Laubach S, Laubach S, et al. Iron-oxygen vacancy defect centers in PbTiO_3 : Newman superposition model analysis and density functional calculations. *Physical Review B*. 2005;71(13).
46. Lohkämper R, Neumann H, Arlt G. Internal bias in acceptor-doped BaTiO_3 ceramics: Numerical evaluation of increase and decrease. *Journal of Applied Physics*. 1990;68(8):4220-4.
47. Waser R. Bulk Conductivity and Defect Chemistry of Acceptor-Doped Strontium-Titanate in the Quenched State. *Journal of the American Ceramic Society*. 1991;74(8):1934-40.
48. Warren WL, Vanheusden K, Dimos D, Pike GE, Tuttle BA. Oxygen Vacancy Motion in Perovskite Oxides. *Journal of the American Ceramic Society*. 1996;79(2):536-8.
49. Schütz D, Deluca M, Krauss W, Feteira A, Jackson T, Reichmann K. Lone-Pair-Induced Covalency as the Cause of Temperature- and Field-Induced Instabilities in Bismuth Sodium Titanate. *Advanced Functional Materials*. 2012;22(11):2285-94.
50. Glaum J, Simons H, Acosta M, Hoffman M. Tailoring the Piezoelectric and Relaxor Properties of $(\text{Bi}_{1/2}\text{Na}_{1/2})\text{TiO}_3$ - BaTiO_3 via Zirconium Doping. *Journal of the American Ceramic Society*. 2013;96(9):2881-6.

Figure and Table Caption List:

Table 1: Ionic transport numbers of the investigated Fe-doped NBT and NBT-6BT compositions.

Figure 1: XRD patterns of undoped and Fe-doped (a) NBT and (b) NBT-6BT.

Figure 2: SEM images of (a) pure NBT and (b) NBT-6BT in comparison to (c) 4 mol% Fe-doped NBT and (d) 4 mol% Fe-doped NBT-6BT.

Figure 3: Grain size of Fe-doped NBT and NBT-6BT as a function of Fe-doping content.

Figure 4: Electron paramagnetic resonance spectra measured at 9.39 GHz of Fe-doped NBT (a) and NBT-6BT (b) as a function of Fe-doping content. The spectral contributions attributed to Fe^{3+} -oxygen vacancy complexes (black diamond) and the Fe-containing impurity phase (green circle) are marked.

Figure 5: Impedance plots for Fe doped and undoped (a) NBT and (b) NBT-6BT at 500°C. (c) Impedance comparison of 1% Fe-doped NBT and NBT-BT at 500°C.

Figure 6: Arrhenius plots for the bulk response of Fe doped and undoped (a) NBT and (b) NBT-6BT.

Figure 7: Polarization vs applied electric field at room temperature for a) NBT based material and b) NBT-BT based material of this study.

Table 1: Ionic transport numbers of the investigated Fe-doped NBT and NBT-6BT compositions.

Composition	t_{ion} at 700°C	t_{ion} at 800°C
1% Fe NBT	0.93	0.90
2% Fe NBT	0.89	0.90
1% Fe NBT-BT	0.07	0.07
2% Fe NBT-BT	0.83	0.84
3% Fe-NBT-BT	0.83	0.83

